Nanoscale

PAPER

View Article Online
View Journal | View Issue

Cite this: *Nanoscale*, 2024, **16**, 6495

Effect of solvent quality and sidechain architecture on conjugated polymer chain conformation in solution†

Guorong Ma, [a] Zhaofan Li,[b] Lei Fang, [c] Wenjie Xia [b] and Xiaodan Gu *[a]

Conjugated polymers (CPs) are solution-processible for various electronic applications, where solution aggregation and dynamics could impact the morphology in the solid state. Various solvents and solvent mixtures have been used to dissolve and process CPs, but few studies have quantified the effect of solvent quality on the solution behavior of CPs. Herein, we performed static light scattering and small-angle X-ray scattering combined with molecular dynamics (MD) simulation to investigate CP solution behaviors with solvents of varying quality, including poly(3-alkylthiophene) (P3ATs) with various sidechain lengths from $-C_4H_9$ to $-C_{12}H_{25}$, poly[bis(3-dodecyl-2-thienyl)-2,2′-dithiophene-5,5′-diyl] (PQT-12) and poly[2,5-bis(3-dodecylthiophen-2-yl)thieno[3,2-*b*]thiophene] (PBTTT-12). We found that chlorobenzene is a better solvent than toluene for various CPs, which was evident from the positive second virial coefficient A_2 ranging from 0.3 to 4.7 × 10^{-3} cm^3 mol g^{-2} towards P3ATs. For P3ATs in non-polar solvents, longer sidechains promote more positive A_2, indicating a better polymer–solvent interaction, wherein A_2 for toluene increases from −5.9 to 1.4 × 10^{-3} cm^3 mol g^{-2}, and in CB, A_2 ranges from 1.0 to 4.7 × 10^{-3} cm^3 mol g^{-2} when sidechain length increases from $-C_6H_{13}$ to $-C_{12}H_{25}$. Moreover, PQT-12 and PBTTT-12 have strong aggregation tendencies in all solutions, with an apparent positive A_2 (~0.5 × 10^{-3} cm^3 mol g^{-2}) due to multi-chain aggregates and peculiar chain folding. These solvent-dependent aggregation behaviors can be well correlated to spectroscopy measurement results. Our coarse-grained MD simulation results further suggested that CPs with long, dense, and branched sidechains can achieve enhanced polymer–solvent interaction, and thus enable overall better solution dispersion. This work provides quantitative insights into the solution behavior of conjugated polymers that can guide both the design and process of CPs toward next-generation organic electronics.

Received 11th November 2023,
Accepted 21st January 2024

DOI: 10.1039/d3nr05721f

rsc.li/nanoscale

1. Introduction

Numerous innovative electronic devices have demonstrated novel applications with remarkable efficiency, sensitivity, and mobility, such as organic photovoltaics (OPV),[1] organic electrochemical transistors (OECTs),[2] and organic field effect transistors (OFETs).[3] The active layer of these devices is commonly composed of organic materials, including small molecules or conjugated polymers (CPs).[4] CPs offer a host of advantages, such as intrinsic stretchability, environmental stability, adjustable energy levels, and solution processability, owing to their versatile chemical structure through coupling synthesis.[5] Generally, CPs feature continuous delocalized electron distribution along their backbone for efficient charge transport, alongside short dispersed sidechains to enhance solubility.[6] In practice, it is observed that long sidechains and high temperatures, in addition to the choice of suitable solvents, improve the solubility of many CPs.[7] Nonetheless, a systematic comparison in this regard to elucidate the solvent quality effect is currently lacking.

To preserve conductive pathways along the backbone, chain conformation is crucial where a rigid and coplanar backbone is ideal.[7,8] The way CPs are arranged in the solid state significantly affects their electronic and optoelectronic properties, making solution behavior a critical aspect for processing CP-based devices. The behavior of polymer chains in the solution phase directly impacts their packing in the solid state. This includes factors such as solubility, chain conformation, and interactions between polymer chains. CPs can be dispersed in a solution to form small aggregates, fully dissolved single chains, or a mixture of both.[9] These heterogeneous states of

[a]*School of Polymer Science and Engineering, The University of Southern Mississippi, Hattiesburg, MS, 39406, USA. E-mail: xiaodan.gu@usm.edu*
[b]*Department of Aerospace Engineering, Iowa State University, Ames, IA 50011, USA*
[c]*Department of Chemistry, Texas A&M University, College Station, TX 77843, USA*

† Electronic supplementary information (ESI) available: Sample preparation, dn/dc measurement, HSP calculation, DSC measurements, scattering, and spectroscopy measurements of the samples in solution and solid states. Additional coarse grain modelling data. See DOI: https://doi.org/10.1039/d3nr05721f

CPs in the solution depend on solvent quality and temperature, yielding drastically different particle sizes and dynamics.[9] Upon aging, doping, or adding antisolvents, CPs can form multichain aggregates from dissolved a solution, where the shape of aggregates can vary from long fibers to spherical aggregates.[10–12] CP chain conformation can be probed *via* small-angle scattering, using X-ray, neutron, or laser light.[12–14] Overall, CP chain conformation and aggregation behavior in the solution can be effectively controlled by solvent selection besides optimal processing conditions.

Numerous studies have concentrated on manipulating chain conformation and pre-aggregate formation by employing a range of solvents or solvent mixtures.[15] These solvents possess diverse characteristics including solubility, toxicity, boiling point, viscosity, and polarity.[16,17] Newbloom *et al.* investigated the gelation of poly(3-alkylthiophene)s (P3ATs) in a mixture of good and poor solvents.[18] They found that for P3HT in dichlorobenzene, more poor-solvent *n*-dodecane results in smaller, abundant fiber formation and better electrical conductivity. Chang *et al.* investigated the solvent-addictive acetone effect on the precursor solution of P3HT in chloroform.[19] The 4-fold increase in charge mobility is attributed to the acetone–chloroform complex, which has a lower evaporation rate. Lee *et al.* investigated the chain conformation of a donor–acceptor fused thiophene–diketopyrrolopyrrole copolymer (PTDPPTFT4) in a solvent mixture of tetrahydronaphthalene and *p*-xylene.[20] The increase of *p*-xylene leads to a higher degree of aggregation along with a more oriented film due to non-polar and weak interactions of *p*-xylene with the polar backbone. The rigid aggregation fraction was confirmed by SAXS. Kwok *et al.* studied the chain conformation of isoindigobithiophene-based polymer (PII-2T) in a chlorobenzene and decane mixture.[21] All polymer solutions contain fibril and dispersed single chains at various concentrations (1–20 mg ml^{-1}), leading to complex modeling, which requires careful data analysis for solution scattering. Xi *et al.* investigated the morphology of poly[2,5-(2-octyldodecyl)-3,6-diketopyrrolopyrrole-*alt*-5,5-(2,5-di(thien-2-yl))thieno[3,2*b*]thiophene] (DPPDTT) aggregates using small-angle neutron scattering.[11] By adding 5–20 v% poor solvent methanol and dimethyl sulfoxide (DMSO) into good solvent chloroform, they found chain rigidity change upon adding poor solvents, depending on the polarity of poor solvents. However, in terms of the interaction between the polymer and solvent, these works did not focus their discussions on the solvent quality.

Traditionally, solvent quality can be estimated by Hansen solubility parameters (HSP), where the cohesive energy between the solute and the solvent can be separated into dispersion, polarity, and hydrogen bonds.[22] It has been used to optimize the solvent for CPs[17,23] and predict the phase separation of the donor and the acceptor blend of OPV devices.[7,24] Machui *et al.* measured the HSP values of P3HT and PCBM and found that the semicrystalline nature of P3HT limits the HSP prediction.[25] Zhao *et al.* used different HSP values to differentiate the cohesive interaction to solvents between the backbone and the sidechain and found that the backbone has more polarity and dispersion attributions than alkyl sidechains.[26] However, the HSP values are empirical and this measurement requires several grams of materials and is often time-consuming.[22] On the other hand, static light scattering (SLS) can be used to probe solvent quality in dilute solutions, which only requires a small amount of the sample and is readily accessible compared to small-angle neutron and X-ray scattering techniques. Recently Liu *et al.* studied the effect of solvent quality on the aggregate shape of DPP–DTT in chloroform.[27] A negative second virial coefficient (-4.4–$+0.5 \times 10^{-6}$ ml^3 mol g^{-2}) was obtained, which indicated that chloroform was a bad solvent despite the dispersion of DPP–DTT in it. Liu *et al.* measured fractal dimensions of the poly(9,9-dioctylfluorene) (PFO) chain solution in chlorobenzene, toluene, tetrahydrofuran, and chloroform.[28] PFO forms aggregates in all solvents at concentrations above 1.0 mg ml^{-1} despite varying levels of aromaticity. Li *et al.* investigated the effect of chloroform/toluene on the bulky polydiarylfluorene (P7DPF) solution.[29] By using SLS, the fractal dimensions of the aggregates increased from 0.62 to 1.76 as the poor solvent toluene volume fraction increased from 0.5 to 1.0. However, what is the solvent quality for other CPs and how does the solvent quality impact the chain conformation is not well known.

In this work, we studied a series of thiophene-derived model CPs in various solvents. These CPs include poly(3-alkylthiophenes) (P3ATs) with various sidechain lengths, ranging from $-C_4H_9$ to $-C_{12}H_{25}$ (P3BT to P3DDT), PQT-12 and PBTTT-12, and thiophene-derived donor–accepter CP PffBT4T–C9C13. We performed dynamics light scattering (DLS), static light scattering (SLS), UV-vis, and small angle X-ray scattering (SAXS). The second virial coefficient (A_2) can be obtained by constructing a Debye plot from the SLS experiment. We found that chlorobenzene is a better solvent than toluene and chloro-

Xiaodan Gu

Xiaodan Gu received his PhD from the Department of Polymer Science and Engineering at the University of Massachusetts Amherst in 2014. Subsequently, he did a post-doctoral study at Stanford University and SLAC National Accelerator Laboratory. Since 2017, he has been a Nina Bell Suggs Endowed Associate Professor from the School of Polymer Science and Engineering at the University of Southern Mississippi. His current research interest revolves around various fundamental polymer physics phenomena related to conjugated polymers and their derivative devices. His group studies the structure, dynamics, and morphology of conjugated polymers and aims to link their molecular structures to their macroscopic properties through advanced metrology with an emphasis on scattering techniques.

form towards various CPs, where all CPs in chlorobenzene showed a positive A_2. For P3ATs in non-polar solvents such as toluene, a longer alkyl sidechain promotes better polymer–solvent interaction towards non-polar solvents and sidechain and thus higher A_2. Meanwhile, PQT-12 and PBTTT-12, have a stronger tendency to aggregate in all the solvents, with a much smaller negative A_2. A donor–acceptor CP, PffBT4T–C9C13 in chlorobenzene also has a negative A_2 of -2.8×10^{-6} cm^3 mol g^{-2} even at an elevated measurement temperature of 65 °C. We performed coarse-grained molecular dynamics (CG-MD) simulation on CPs with various architectures and grafting density in an implicit solvent with various solvent qualities, and our simulation results suggest that CPs with dense and branched sidechains have better polymer–solvent interaction. Our work provides insights into the solution behavior of conjugated polymers that can guide both the design and process of CPs toward next-generation organic electronics.

2. Experiment

2.1. Materials

All P3ATs (Rieke metals), PQT-12 (Sigma-Aldrich), PBTTT-12 (Sigma-Aldrich), and PffBT4T–C9C13 (Ossila, M_w = 123 kDa) were used as received. All the solvents (toluene, chlorobenzene, tetrahydrofuran, and chloroform) were purchased from Sigma-Aldrich and filtered through a 0.2 μm PTFE filter before use. CPs were first dissolved at 80 °C in various solvents overnight for better dispersion, then cooled to measure the temperature for the test.

2.2. UV-vis

UV-vis spectroscopy was performed on a Cary 5000 UV-Vis-NIR spectrophotometer (Agilent Technologies) with a 3 mm optical path quartz cuvette.

2.3. Dynamic light scattering (DLS) and static light scattering (SLS)

Dynamic light scattering and static light scattering were performed on a Brookhaven BI-200SM research goniometer with a BI-APD avalanche photodiode detector and a 35 mW, 633 nm laser source with 90°-angle geometry. Solutions were held in a capped glass tube and the temperature was controlled using a cyclic intracooler with a temperature variation of ±1 °C.

In DLS, an autocorrelation function, $C(t)$ was calculated based on the fluctuation signal:

$$C(t) = Ae^{-2\Gamma t} + B$$

wherein A is the optical constant through the instrument design, Γ is the relaxation of the fluctuation, t is time and B is the constant background. Γ and q are defined as $\Gamma = Dq^2$ and scattering vector $q = \frac{4\pi n_0}{\lambda_0}\sin\left(\frac{\theta}{2}\right)$. The size distribution of the particles was analyzed by the Brookhaven software using cumulants analysis.

In SLS, the Debye plot was constructed based on static scattering intensity:

$$\frac{H_c}{R(q)} = \frac{1}{M_w}\left(1 + \frac{1}{3}q^2{R_g}^2 + \cdots\right) + 2A_2c$$

where $H = \frac{4\pi^2}{N_A\lambda^4}n^2\left(\frac{dn}{dc}\right)^2$, and $R(q) = \frac{I_s(\theta)r^2}{I_0V_s(\theta)} = \frac{I_{solution}/I_{0,solution} - I_{solvent}/I_{0,solvent}}{I_{std}/I_{0,std}}R_{std}$. The differential refractive index, $\frac{dn}{dc}$, was measured and listed in ESI under Table S3.†

2.4. Small-angle X-ray scattering (SAXS)

SAXS experiments were performed at the NSLS-II 12-ID located at Brookhaven National Laboratory (BNL). Polymers were dissolved in toluene or chlorobenzene at a concentration of 8 mg ml^{-1}. The solution was sealed in a thin-wall capillary tube with a tube diameter of 1 mm. 16.1 keV X-ray was used to minimize the absorption from chlorinated solvents and two sample-to-detector distances were used to cover the range of the scattering wavevector q from 0.01 to 3.0 Å^{-1}. The solution temperature was controlled using Lake Shore Cryotronics equipment with an accuracy of ±1 °C. Background scattering was subtracted carefully in Igor WaveMetrics along with the Nika package. The model fitting was performed in SasView 5.0 software.

2.5. CG-MD simulations

We employed generic bead-spring CG models of CPs and MD simulations to systematically explore the conformational behaviors of CP chains in dilute solutions. We model CPs based on various branched chain structures as depicted in Fig. 4a, aiming to represent a broad range of CPs. Specifically, the CG model comprises a linear backbone composed of N_{bb} monomers, represented by cyan beads. The key feature of our CG model lies in the diverse sidechain architectures (orange beads) appended to this backbone, enabling a systematic examination of the impact of different sidechain arrangements on the conformational behavior of the polymer. In this study, all physical quantities within our system are expressed in reduced Lennard-Jones (LJ) units. These units include ε, σ, and m for energy, length, and mass, respectively. Additionally, time, temperature, and pressure are defined by τ, ε/k_B, and ε/σ^3, respectively, where $\tau = \sqrt{m\sigma^2/\varepsilon}$ with k_B representing the Boltzmann constant. Importantly, these reduced units are amenable to straightforward conversion into the physical units applicable to real-world laboratory measurements of polymer materials. Similar models have been widely harnessed to investigate a broad spectrum of dynamic, conformational, structural, and mechanical properties exhibited by CPs, both in melt and solution states.[30]

Significantly, to account for polymer–solvent interactions, we introduced a dimensionless parameter denoted as λ, which serves as a valuable tool for qualitatively capturing the varying quality of the solvent in a solution state. By adjusting the para-

meter λ across the particles, we can effectively modulate the 'solvent quality'. Specifically, when λ is set to 0, the polymer should be in an ideal and good solvent, characterized by purely repulsive interactions. However, as we incrementally increase the value of λ, we could systematically decrease solvent quality, attributable to the introduction of attractive forces among the polymer chain (see ref. 31 for a detailed study of the relationship between the solvent quality and parameter λ).

3. Results and discussion

First, we studied solvent and polymer interactions for polythiophenes with different lengths of the sidechain, ranging from $-C_4H_9$ to $C_{12}H_{25}$ (Fig. 1a). Two commonly used solvents, chlorobenzene (CB) and toluene (Tol) were studied. Upon heating, all the P3ATs formed clear bright orange solutions. When cooled to 20 °C, all the absorption spectra for polythiophenes (Fig. 1b and c, and S1†) were similar. However, P3BT, PQT-12, and PBTTT-12 solutions became darker upon cooling in both CB and Tol, with an absorption tail above 600 nm, which interacts with the He–Ne laser. This is typically referred to as the absorption of aggregates where the backbone is stacked closer[32] and this aggregation was further confirmed by DLS. The delayed autocorrelation function decay was caused by the slow Brownian motion of large objects and the particle size was converted by the Stokes–Einstein equation (Fig. 1d–g). The peak at around 10 nm in diameter results from the random Brownian motion of the dissolved single chain. However, P3BT, PQT-12, and PBTTT-12 solutions showed extra peaks larger than 100 nm in the histogram of particle size (Fig. 1d and g, and S2†), indicating the existence of large multi-chain aggregates. This strong aggregation tendency was expected as P3BT has the shortest sidechain ($-C_4H_9$) and PQT-12 and PBTTT-12 have better charger device performance,[33] where close π–π stacking overwhelmed entropy-favored dissolving-processing due to the insufficient sidechain length and reducing sidechain graft density.

Then, we performed SLS on dilute solutions of CPs with the concentration ranging from 0.2 to 1.0 mg ml^{-1}. The SLS setup is illustrated in Fig. 2a, where the light scattering intensity of

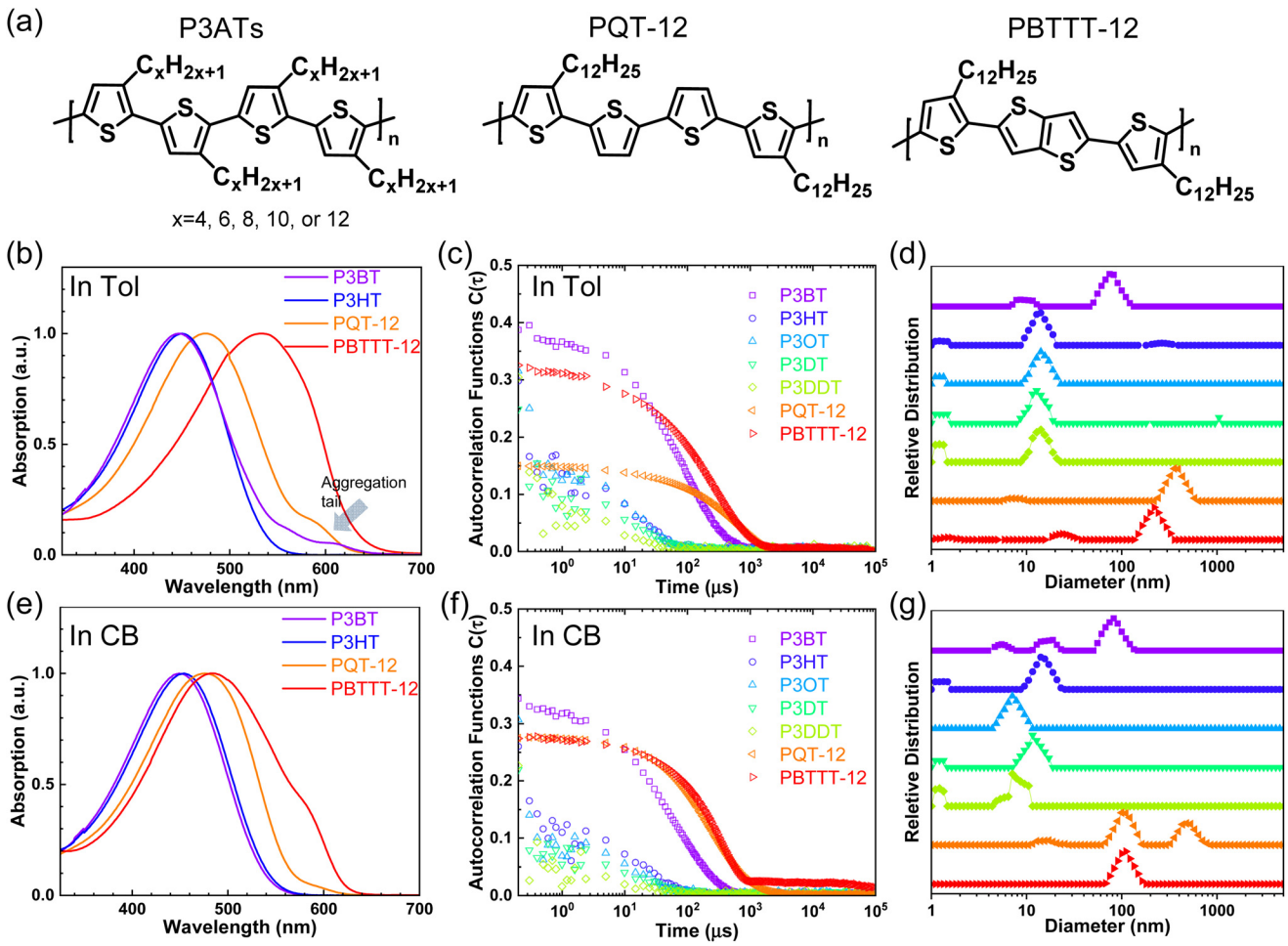

Fig. 1 (a) Chemical structures of P3ATs, PQT-12, and PBTTT-12. UV-vis absorption spectra of CPs in toluene (b) and CB (e) at 20 °C. Autocorrelation curves of CPs in toluene (c) and CB (f) from DLS measurements at 20 °C. Size distribution of CPs in toluene (d) and CB (g) from DLS measurements.

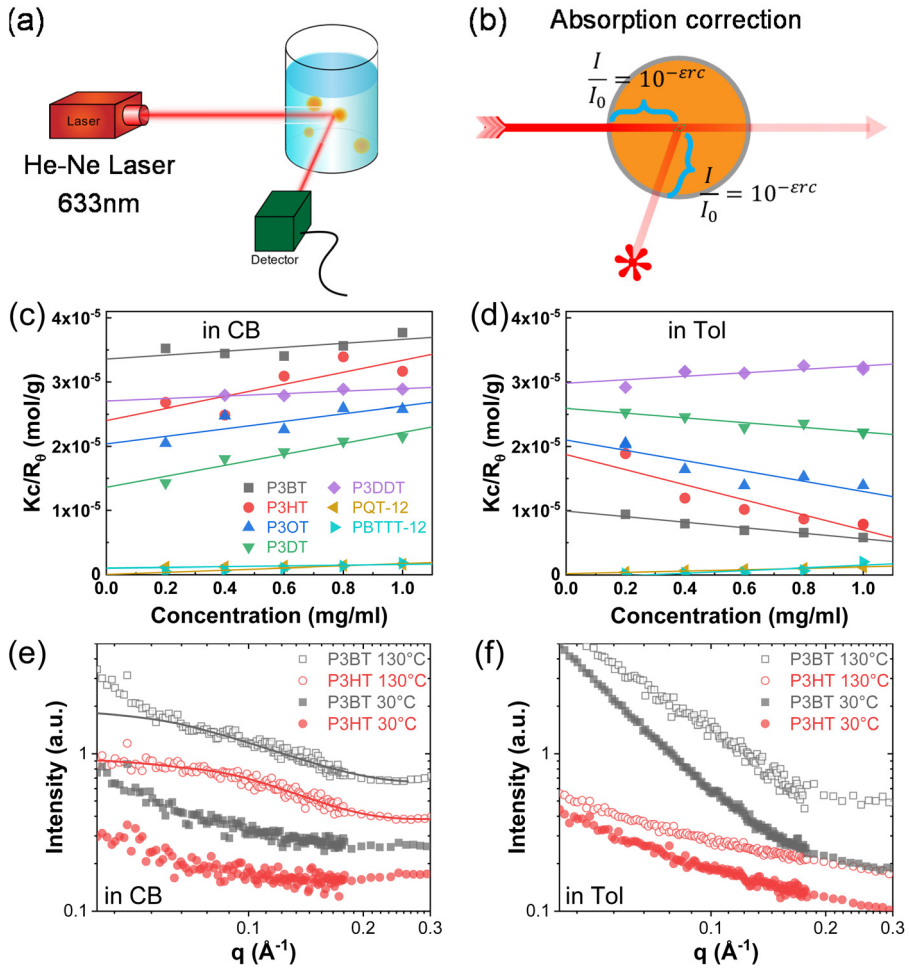

Fig. 2 (a) An illustration of the setup of static light scattering. (b) The principle of absorption correction is based on Lambert-Beer's law. (c and d) Debye plot of CPs in CB (c) and in toluene(d) at 20 °C. Absorption correction was applied to PQT-12, PBTTT-12 in CB and P3BT, PQT-12, and PBTTT-12 in Tol. (e and f) SAXS data of P3BT and P3HT in CB (e) and Tol (f) at 30 °C (closed symbol) and 130 °C (open symbol). Continuous lines are fitting curves using a flexible cylinder model and the scattering profile was shifted vertically for clarity.

different concentration solutions was measured using a photon detector with a 633 nm wavelength filter. Some CP solutions could absorb red light, which could lower the scattering intensity at different angles and cause issues in constructing the Debye plot. Thus, proper absorption correction for those samples is needed, where Lambert–Beer law was used. The light path is illustrated in Fig. 2b and the Debye plot is plotted in Fig. 2c and d, and S7.† The linear fit yields from the data point in the Debye plot gave A_2, half of the slope, which is listed in Table 2. We found that CB is a better solvent for all P3ATs compared to toluene, THF, and chloroform, as all A_2 in CB are positive but some negative in other solvents. As the sidechain length increases, the A_2 in toluene and THF increases, which indicates better polymer–solvent interaction. This is expected as the sidechain mass fraction increases (Table 1) as sidechain length increases, which is more soluble than the rigid backbone of CPs based on the HSP theory (Fig. S6 and Table S4†). To investigate the impact of the side-

Table 1 Summary of the molar masses and sidechain mass fractions of CPs

Name	Alkyl sidechain	M_w (avg), kg mol^{-1}	Dispersity $Đ$	Sidechain mass fraction m_f	Regioregularity
P3BT	–C4H9	41k	2.3	0.41	85%
P3HT	–C6H13	42k	2.0	0.51	90%
P3OT	–C8H17	60k	2.0	0.58	92%
P3DT	–C10H21	62k	2.1	0.64	92%
P3DDT	–C12H25	60k	2.0	0.68	92%
PQT-12	–C12H25	17.5k	3.0	0.51	—
PBTTT-12	–C12H25	60k	3.0	0.53	—

Table 2 A_2 values of CPs in all the solvents at 20 °C

	A_2 ($\times 10^{-3}$ cm^3 mol g^{-2})			
Polymer/solvent	CB	Toluene	THF	Chloroform
P3BT	1.5	−2.2	−7.8	−4.6
P3HT	4.7	−5.9	−4.4	−3.5
P3OT	2.9	−4.0	−3.2	−4.7
P3DT	4.3	−1.9	−1.5	−2.6
P3DDT	1.0	1.4	−3.8	−4.8
PQT-12	0.3	0.5	None	None
PBTTT-12	0.8	−0.5	None	None

chain length on the solvent quality, we conducted a small-angle X-ray scattering (SAXS) analysis to examine the chain conformation of both P3BT and P3HT in CB and Tol. The scattering profiles are depicted in Fig. 2e for the CB solution and Fig. 2f for the Tol solution. It is evident that both polymers form homogenous solutions in both solvents. When the temperature was set at 30 °C in CB, the scattering intensity of both polymers increased in the low-q region, indicating the presence of loose aggregates with a large feature size. At elevated temperatures (130 °C), a Guinier region emerged in the intermediate q range. Notably, the low-q upturn of the intensity was observed in P3BT but not in P3HT, suggesting a more effective dissolution of P3HT with longer side chains. Fitting the curve using the flexible cylinder model allowed us to probe the chain conformation, and the results are detailed in Table 3. The polymer chain conformation aligns well with that of a flexible cylinder, exhibiting a cylinder radius of 1.2 ± 0.4 nm for P3BT and 1.3 ± 0.2 nm for P3HT, indicative of a well-dissolved single chain. In contrast, toluene could only disperse both polymers, since the evidence of single chain scattering or an obvious Guinier plateau regional is missing.[34] This aligns with the solvent quality assessment, affirming that CB serves as a better solubilizing solvent for P3ATs when compared to toluene. Furthermore, the solvent quality can impact the macroscopic spectroscopy, as shown in Fig. S4.† For those dispersed aggregates, the polymer exhibits a red-shifted absorption peak approximately at 610 nm, in addition to the primary absorption at 450 nm for P3BT in toluene.

However, sidechain architecture also played a role as we compared P3HT, PQT-12, and PBTTT-12, where the sidechain mass fraction was similar to that calculated, as shown in Table 1. PQT-12 and PBTTT-12 strongly aggregate and form light-absorbing solutions especially in THF and chloroform, so we only measured A_2 for CPs in CB and toluene. The positive A_2 of PQT-12 and PBTTT-12 is not an indication of a fully dissolved single chain in the solution as this could be achieved by a dedicated self-assembled structure where the sidechain is exposed outside while the backbone is buried inside. This is not surprising as CPs have complex multi-length scale structures in the solution.[7,35] The double-length sidechain and the reduced sidechain grafting density lead to a strong aggregate attendance in all the solvents. This strong aggregation tendency is expected for semicrystalline CPs where PQT-12 and PBTTT-12 are more crystalline in the solid state, as revealed by DSC (Fig. S8†). The negative A_2 of P3HT in toluene suggests bad polymer–solvent interaction, indicating the collapse of the polymer interchains, and interchain aggregation are thermodynamically favorable. This slow and subtle transition can be observed in aging tests over days by DLS (Fig. S9†) and a similar effect has been reported previously.[13,36] After cooling from the hot solution and aging at room temperature, the hydrodynamic diameter of the particle keeps increasing in the P3HT toluene solution but is maintained in the CB solution. Thus, we conclude that CB is the best solvent for all the P3ATs compared to Tol, THF, and chloroform.

We then examined the sidechain architecture's effect on the solvent quality by comparing P3HT, PQT-12, and PBTTT-12. They have similar sidechain fractions but different sidechain lengths, grafting density, and backbone stiffness. PQT-12 and PBTTT-12 strongly aggregate in the solution at room temperature and form a deep red solution (Fig. S1†). The aggregate size is larger than 100 nm in diameter as seen by DLS in the dilute solution (Fig. 1d and g), while the aggregate could be a long fiber, as seen previously.[37] This makes both DLS and SLS harder as the solution strongly absorbs the red light and the thermal lens effect distorts the optical light path.[38] This leads to a significant broadening of the beam path and a distorted transmission beam, as shown in Fig. S10.† Nonetheless, P3HT has better polymer–solvent interaction than its analog PQT-12 and PBTTT-12, with different sidechain architecture.

To explore high-performance CPs, we also examined donor–acceptor CPs PffBT4T–C9C13 in the solvent chlorobenzene. PffBT4T–C9C13 has significant temperature-dependent absorption (Fig. 3b) and aggregation behavior in the solution that has been well-reported.[39] Large aggregates form immediately as the solution cools down and breaks apart gradually at elevated temperatures. The optical absorption of the solution at 633 nm decreases, making SLS possible to probe the solvent quality at a single chain level. Before light absorption correction, the Zimm plot was not meaningful since it gives a negative molar mass. After the light absorption correction, we obtained M_w = 156 kg mol^{-1}, which is comparable to the GPC result ($M_{w,\ GPC}$ = 123 kg mol^{-1}). Interestingly, the $A_2 = -2.8 \times 10^{-6}$ cm^3 mol g^{-2}, which is on the similar magnitude of DPPT

Table 3 Fitting parameters from SAXS on P3BT and P3HT using a flexible cylinder model

Name	Length/nm	Kuhn length/nm	Radius/nm	Fitting error χ^2
P3BT in CB 130 °C	5.3 ± 0.5	5.8 ± 0.6	1.2 ± 0.4	0.22
P3HT in CB 130 °C	3.2 ± 0.6	4.6 ± 0.8	1.3 ± 0.2	0.15

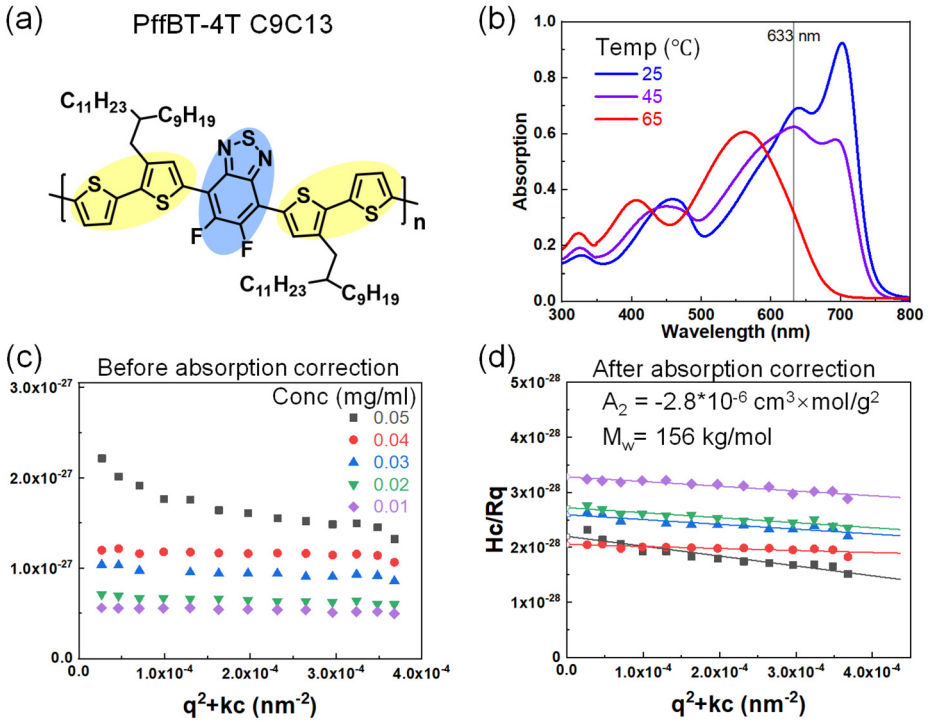

Fig. 3 (a) Chemical structure of PffBT4T–C9C13. The donor part and acceptor part are colored as yellow and blue units, respectively. (b) UV-vis of PffBT4T–C9C13 in CB at various temperatures. The laser wavelength used in the light scattering test is marked in a gray line. (c, and d) SLS of PffBT4T–C9C13 in CB at 65 °C before and after the absorption correction.

in chloroform.[27] This small and negative A_2 showed that CPs have thermodynamically unfavorable polymer–solvent interaction where aggregation is inevitable. However, one A_2 parameter cannot differentiate the interaction between the sidechain and backbone of the solvent, furthermore, there is a lack of synthetically achievable variations of the sidechain. Overall, the complex CP structure with rigid conjugated backbone and flexible sidechain, heterogeneous dynamics between backbone and sidechains, and particularly strong π–π interaction between the backbones lead to peculiar self-assembly behavior of CPs in the solution.

To elucidate the impact of solvent quality and sidechain architecture on CPs in a broader context, we conducted CG-MD simulations to explore four distinct sidechain architectures of CPs representing diverse chemical structures, as shown in Fig. 4a. Specifically, we constructed CPs with (I) short dense sidechains, (II) long and less dense sidechains, (III) dense branched sidechains, and (IV) less dense branched sidechains. The introduction of the solvent quality parameter λ to characterize the polymer–solvent interactions provides a versatile means to fine-tune the solvent quality by adjusting λ among individual particles, where higher λ values correspond to poor solvent quality. In our simulations, we systematically tracked the polymer chain conformational changes and recorded the time-dependent evolution of the radius of gyration (R_g) under varying solvent conditions, while also accounting for the influence of the sidechain architecture, as shown in Fig. 4.

Herein, we consistently observed three distinct stages across all scenarios. For λ values below 0.4, the polymer chain exhibited its largest R_g, indicative of an extended coil conformation, as exemplified in the illustrative representation shown in Fig. 4b. This behavior aligns with the expected characteristics of a chain in a favorable solvent environment. As λ progressively increases, R_g gradually diminishes, reflecting a gradual compaction of the polymer coil within the solution—consistent with the behavior of a fully dissolved chain. Conversely, when λ exceeds 0.6, R_g reaches a near minimum, signaling the collapse of the polymer chain into a compact single conformation, as demonstrated in the illustrative representation. Notably, as λ transitions from 0.4 to 0.6, R_g experiences a rapid decrease, highlighting a notable phase transition that becomes increasingly well-defined with increasing chain length N_{bb}. Moreover, four distinct polymer chains with different sidechain architectures were simulated to extrapolate the θ condition to quantitively compare the solvent quality and chain conformation. When the polymer chain is in θ state, polymer chains are free to coil and extend in the solution which can be described by a random walk in 3D space, where the normalized coil size $R_g^2/(N-1)$ is independent of the polymer chain length N. Thus, we can find the θ point with the intersection of the four chains of different lengths in the λ coordinate. The larger the λ_θ, the worse the solvent where the polymer chain can form a free coil, and thus this polymer is more soluble at a given solvent quality parameter λ. Hence, we conclude that Type III exhibits the most favorable solvent

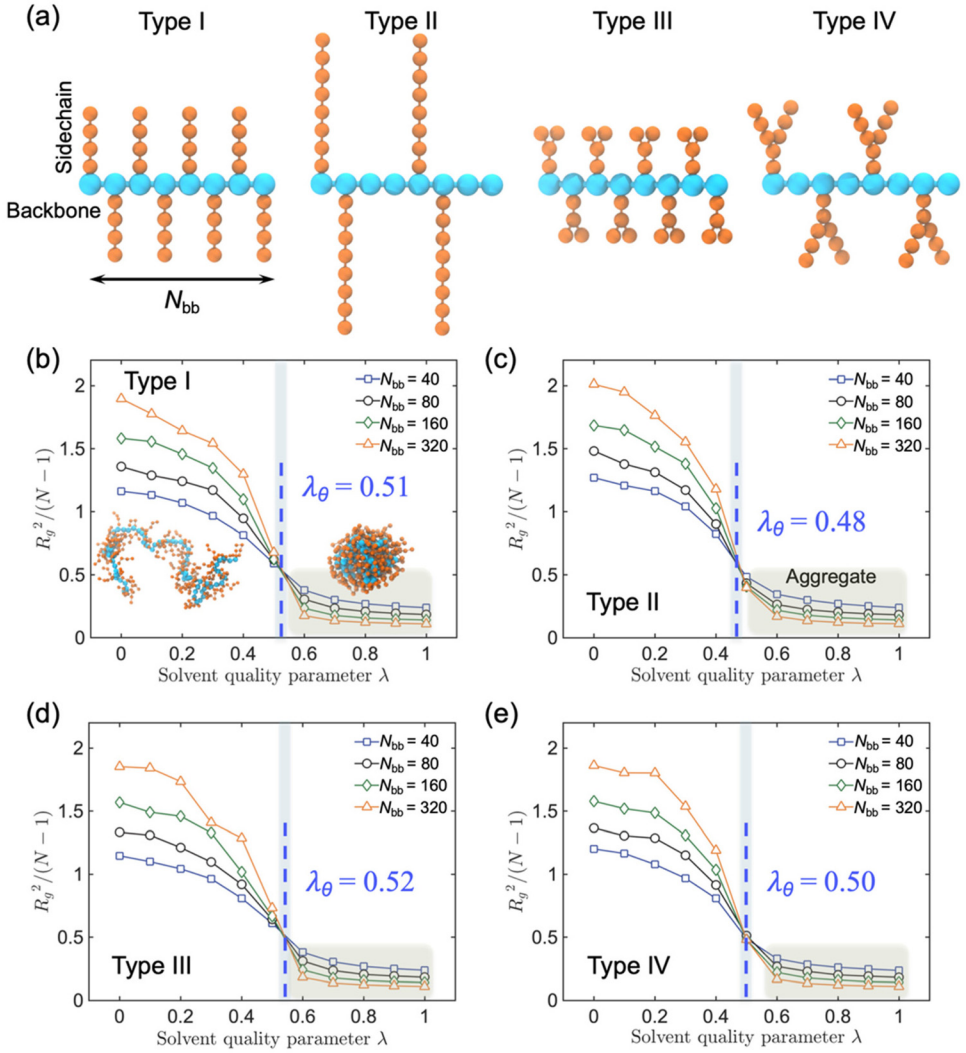

Fig. 4 CG MD simulation results. (a) Polymer architectures of 4 types of CPs. The backbone and sidechain are represented as beads P1 and P2. (b–e) Reduced R_g of the polymer chain as a function of the solvent quality parameter λ for type I to IV. A lower value of λ corresponds to better solvent quality. The location of the θ point is indicated by the blue dashed line.

quality, owing to its higher density and branched configuration of sidechains.

We further explored other analogs of Type II and V, Type III and VI (Fig. S11†), wherein slight variations were introduced in terms of the sidechain distribution along the backbone and sidechain branching position. However, our observations did not reveal any notable distinctions in λ_θ between Type II and VI, Type III and V. These findings suggest that the process of CP dissolution is primarily governed by entropy considerations, with a greater emphasis on the quantity of the sidechain ends proving to be more influential in this context.[40] A parallel trend is also evident at higher temperatures, wherein polymer chains characterized by longer, denser, and more extensively branched sidechains exhibit enhanced solubility, as shown in Fig. S12.† Consistent with the trends observed for R_g, we discerned a parallel pattern in response to variations in the solvent quality for both the persistence length (L_p), which quantifies chain rigidity, and the end-to-end distance (R_{ee}), a parameter commonly used to characterize the polymer chain conformational bends, as depicted in Fig. S13 and S14,† respectively.

To gain a deeper insight into the molecular-level shape of the polymer chain under various solvent conditions, we further examined the shape descriptor known as relative shape anisotropy κ^2, which describes the degree of anisotropy in the chain's shape, specifically regarding its tendency toward rod-like ($\kappa^2 = 1$), planar symmetric ($\kappa^2 = 0.25$), or spherical configurations ($\kappa^2 = 0$).[41] As shown in Fig. S15,† κ^2 exhibits fluctuations within the range of 0.1 to 0.2, remaining relatively stable in a good solvent ($0 < \lambda < 0.4$) across all six types of polymer chains. This stability suggests some level of elongation or asymmetry in the molecular structure, with minimal influence from the sidechain architecture. Conversely, as the solvent quality deteriorates ($0.6 < \lambda < 1.0$), κ^2 decreases significantly towards zero, signaling the onset of the polymer chain aggregation.

4. Conclusion

To conclude, we measured the second virial coefficient A_2 by static light scattering to quantify solvent quality on a series of CP solutions and investigated the effects of the sidechain volume fraction, sidechain architecture, and backbone architecture on optical absorption, particle size, and chain conformation in the solution state. We studied (1) P3ATs with various sidechain lengths, from C4 to C12, (2) two P3HT's analogous PQT-12 and PBTTT-12, and (3) PffBT4T–C9C13, in a variety of solvents. We found that chlorobenzene is a better solvent than toluene and chloroform towards various CPs, where more CPs have positive A_2 in CB only. For P3ATs in non-polar solvents such as toluene, longer sidechain promotes better polymer–solvent interaction towards alkyl sidechains and thus higher A_2. Besides the sidechain fraction, sidechain architecture also impacts the aggregation tendency. For example, PQT-12 and PBTTT-12 have a stronger tendency to aggregate in all the solvents, despite having a similar sidechain volume ratio to P3HT. Meanwhile, backbone architecture also influences the solvent quality and aggregation tendency. A donor–acceptor CP, PffBT4T–C9C13 in CB also has a negative A_2 at 65 °C. We performed CG molecular dynamics simulation on CPs with various backbones and sidechain architectures in an implicit solvent with various solvent qualities, which suggests that CPs with dense and branched sidechains have stronger polymer–solvent interaction and better solubility. Overall, our study provides quantitative insight into the design and processing of CPs from a polymer–solvent interaction perspective.

Author contributions

X. G. and L. F. conceived and directed the project. All experiments were done and analyzed by G. M. Simulation was performed by Z. L. under the guidance of W. X. The manuscript was written by G. M. with input from all the authors. All authors have revised and approved the final version of the manuscript.

Conflicts of interest

The authors declare no competing financial interest.

Acknowledgements

This work was financially supported by the U.S. National Science Foundation (NSF) under award numbers 2003733, 2004133, 2304968, and 2304969. Z. L. and W. X. acknowledged the support from NSF Award No. CMMI-2237063. We thank BNL beamline scientists Wasik Patryk and Guillaume Freychet for their help during the SAXS measurement. This research used resources 12-ID of the National Synchrotron Light Source II, a U.S. Department of Energy (DOE) Office of Science User Facility operated for the DOE Office of Science by Brookhaven National Laboratory under Contract No. DE-SC0012704.

References

1 R. Zeng, L. Zhu, M. Zhang, W. Zhong, G. Zhou, J. Zhuang, T. Hao, Z. Zhou, L. Zhou, N. Hartmann, *et al.*, All-polymer organic solar cells with nano-to-micron hierarchical morphology and large light receiving angle, *Nat. Commun.*, 2023, **14**(1), 4148, DOI: **10.1038/s41467-023-39832-4**; L. Zhu, M. Zhang, J. Xu, C. Li, J. Yan, G. Zhou, W. Zhong, T. Hao, J. Song, X. Xue, *et al.*, Single-junction organic solar cells with over 19% efficiency enabled by a refined double-fibril network morphology, *Nat. Mater.*, 2022, **21**(6), 656–663, DOI: **10.1038/s41563-022-01244-y**.

2 J. Rivnay, S. Inal, A. Salleo, R. M. Owens, M. Berggren and G. G. Malliaras, Organic electrochemical transistors, *Nat. Rev. Mater.*, 2018, **3**(2), 1–14, DOI: **10.1038/natrevmats.2017.86**.

3 X. Yu, L. Chen, C. Li, C. Gao, X. Xue, X. Zhang, G. Zhang and D. Zhang, Intrinsically Stretchable Polymer Semiconductors with Good Ductility and High Charge Mobility through Reducing the Central Symmetry of the Conjugated Backbone Units, *Adv. Mater.*, 2023, **35**(17), e2209896, DOI: **10.1002/adma.202209896**; J. G. Ibanez, M. E. Rincon, S. Gutierrez-Granados, M. Chahma, O. A. Jaramillo-Quintero and B. A. Frontana-Uribe, Conducting Polymers in the Fields of Energy, Environmental Remediation, and Chemical-Chiral Sensors, *Chem. Rev.*, 2018, **118**(9), 4731–4816, DOI: **10.1021/acs.chemrev.7b00482**.

4 J. R. Reynolds, B. C. Thompson and T. A. Skotheim, *Conjugated Polymers: Properties, Processing, and Applications*, CRC press, 2019. DOI: **10.1201/9780429190520**.

5 N. A. Kukhta and C. K. Luscombe, Gaining control over conjugated polymer morphology to improve the performance of organic electronics, *Chem. Commun.*, 2022, **58**(50), 6982–6997, DOI: **10.1039/d2cc01430k**.

6 T. M. Swager, 50th Anniversary Perspective: Conducting/Semiconducting Conjugated Polymers. A Personal Perspective on the Past and the Future, *Macromolecules*, 2017, **50**(13), 4867–4886, DOI: **10.1021/acs.macromol.7b00582**.

7 Y. C. Xu, L. Ding, Z. F. Yao, Y. Shao, J. Y. Wang, W. B. Zhang and J. Pei, Conjugated Polymers in Solution: A Physical Perspective, *J. Phys. Chem. Lett.*, 2023, **14**(4), 927–939, DOI: **10.1021/acs.jpclett.2c03600**.

8 G. R. Ma, M. W. Leng, S. Li, Z. Q. Cao, Y. R. Cao, D. P. Tabor, L. Fang and X. D. Gu, Robust chain aggregation of low-entropy rigid ladder polymers in solution, *J. Mater. Chem. C*, 2022, **10**(37), 13896–13904, DOI: **10.1039/d2tc00761d**.

9 D. P. Wang, Y. Yuan, Y. Mardiyati, C. Bubeck and K. Koynov, From Single Chains to Aggregates, How Conjugated Polymers Behave in Dilute Solutions,

Macromolecules, 2013, **46**(15), 6217–6224, DOI: **10.1021/ma4011523**.

10 Y. Wu, Z. C. Ding, Q. Zhang, X. Liang, H. Yang, W. L. Huang, Y. L. Su, Y. Zhang, H. L. Hu, Y. C. Han, *et al.*, Increasing H-Aggregates via Sequential Aggregation to Enhance the Hole Mobility of Printed Conjugated Polymer Films, *Macromolecules*, 2022, **55**(19), 8609–8618, DOI: **10.1021/acs.macromol.2c01701**; R. Traiphol, N. Charoenthai, T. Srikhirin, T. Kerdeharoen, T. Osotchan and T. Maturos, Chain organization and photophysics of conjugated polymer in poor solvents: Aggregates, agglomerates and collapsed coils, *Polymer*, 2007, **48**(3), 813–826, DOI: **10.1016/j.polymer.2006.12.003**; Y. C. Li, K. B. Chen, H. L. Chen, C. S. Hsu, C. S. Tsao, J. H. Chen and S. A. Chen, Fractal aggregates of conjugated polymer in solution state, *Langmuir*, 2006, **22**(26), 11009–11015, DOI: **10.1021/la0612769**.

11 Y. Xi, C. M. Wolf and L. D. Pozzo, Self-assembly of donor-acceptor conjugated polymers induced by miscible 'poor' solvents, *Soft Matter*, 2019, **15**(8), 1799–1812, DOI: **10.1039/c8sm02517g**.

12 T. Q. Nguyen, V. Doan and B. J. Schwartz, Conjugated polymer aggregates in solution: Control of interchain interactions, *J. Chem. Phys.*, 1999, **110**(8), 4068–4078, DOI: **10.1063/1.478288**.

13 N. Kleinhenz, C. Rosu, S. Chatterjee, M. Chang, K. Nayani, Z. Z. Xue, E. Kim, J. Middlebrooks, P. S. Russo, J. O. Park, *et al.*, Liquid Crystalline Poly(3-hexylthiophene) Solutions Revisited: Role of Time-Dependent Self-Assembly, *Chem. Mater.*, 2015, **27**(7), 2687–2694, DOI: **10.1021/acs.chemmater.5b00635**.

14 Y. C. Li, C. Y. Chen, Y. X. Chang, P. Y. Chuang, J. H. Chen, H. L. Chen, C. S. Hsu, V. A. Ivanov, P. G. Khalatur and S. A. Chen, Scattering study of the conformational structure and aggregation behavior of a conjugated polymer solution, *Langmuir*, 2009, **25**(8), 4668–4677, DOI: **10.1021/la803339f**; B. J. Schwartz, Conjugated polymers as molecular materials: how chain conformation and film morphology influence energy transfer and interchain interactions, *Annu. Rev. Phys. Chem.*, 2003, **54**, 141–172, DOI: **10.1146/annurev.physchem.54.011002.103811**; G. W. Heffner, D. S. Pearson and C. L. Gettinger, Characterization of poly (3-octylthiophene). I: Molecular characterization in dilute solution, *Polym. Eng. Sci.*, 2004, **35**(10), 860–867, DOI: **10.1002/pen.760351008**.

15 H. Zhang, T. Li, B. Liu, T. N. Ma, L. Huang, Z. M. Bai and D. Lu, Effect and Mechanism of Solvent Properties on Solution Behavior and Films Condensed State Structure for the Semi-rigid Conjugated Polymers, *Chin. J. Polym. Sci.*, 2021, **39**(7), 796–814, DOI: **10.1007/s10118-021-2555-6**; M. Moris, M. P. Van den Eede, G. Koeckelberghs, O. Deschaume, C. Bartic, K. Clays, S. Van Cleuvenbergen and T. Verbiest, Solvent Role in the Self-Assembly of Poly(3-alkylthiophene): A Harmonic Light Scattering Study, *Macromolecules*, 2021, **54**(5), 2477–2484, DOI: **10.1021/acs.macromol.0c02544**; M. Da Pian, M. Maggini, G. J. Vancso, V. Causin and E. M. Benetti, Assembly of poly-3-(hexylthiophene) nanocrystals in marginal solvent: The role of PCBM, *Eur. Polym. J.*, 2018, **109**, 222–228, DOI: **10.1016/j.eurpolymj.2018.09.049**; B. Morgan and M. D. Dadmun, The importance of solvent quality on the modification of conjugated polymer conformation and thermodynamics with illumination, *Soft Matter*, 2017, **13**(15), 2773–2780, DOI: **10.1039/c6sm02631a**.

16 J. K. Li, M. Y. Shao, M. Yu, W. Zhang, Z. Y. Yang, G. Yu, J. Xu and W. Cui, Revealing the Influences of Solvent Boiling Point and Alkyl Chains on the Adlayer Crystallinity of Furan-Diketopyrrolopyrrole-Thienylene Copolymer at Molecular Level, *Langmuir*, 2020, **36**(1), 141–147, DOI: **10.1021/acs.langmuir.9b02604**.

17 H. Opoku, B. Nketia-Yawson, E. S. Shin and Y. Y. Noh, Organic field-effect transistors processed by an environmentally friendly non-halogenated solvent blend, *J. Mater. Chem. C*, 2018, **6**(3), 661–667, DOI: **10.1039/c7tc04823h**; G. G. Jeon, M. Lee, J. Nam, W. Park, M. Yang, J. H. Choi, D. K. Yoon, E. Lee, B. Kim and J. H. Kim, Simple Solvent Engineering for High-Mobility and Thermally Robust Conjugated Polymer Nanowire Field-Effect Transistors, *ACS Appl. Mater. Interfaces*, 2018, **10**(35), 29824–29830, DOI: **10.1021/acsami.8b07643**; J. K. Keum, K. Xiao, I. N. Ivanov, K. L. Hong, J. F. Browning, G. S. Smith, M. Shao, K. C. Littrell, A. J. Rondinone, E. A. Payzant, *et al.*, Solvent quality-induced nucleation and growth of parallelepiped nanorods in dilute poly(3-hexylthiophene) (P3HT) solution and the impact on the crystalline morphology of solution-cast thin film, *CrystEngComm*, 2013, **15**(6), 1114–1124, DOI: **10.1039/c2ce26666k**; C. Scharsich, R. H. Lohwasser, M. Sommer, U. Asawapirom, U. Scherf, M. Thelakkat, D. Neher and A. Köhler, Control of aggregate formation in poly(3-hexylthiophene) by solvent, molecular weight, and synthetic method, *J. Polym. Sci., Part B: Polym. Phys.*, 2012, **50**(6), 442–453, DOI: **10.1002/polb.23022**.

18 G. M. Newbloom, P. de la Iglesia and L. D. Pozzo, Controlled gelation of poly(3-alkylthiophene)s in bulk and in thin-films using low volatility solvent/poor-solvent mixtures, *Soft Matter*, 2014, **10**(44), 8945–8954, DOI: **10.1039/c4sm00960f**.

19 M. Chang, D. Choi, B. Fu and E. Reichmanis, Solvent based hydrogen bonding: impact on poly(3-hexylthiophene) nanoscale morphology and charge transport characteristics, *ACS Nano*, 2013, **7**(6), 5402–5413, DOI: **10.1021/nn401323f**.

20 W. Y. Lee, G. Giri, Y. Diao, C. J. Tassone, J. R. Matthews, M. L. Sorensen, S. C. B. Mannsfeld, W. C. Chen, H. H. Fong, J. B. H. Tok, *et al.*, Effect of Non-Chlorinated Mixed Solvents on Charge Transport and Morphology of Solution-Processed Polymer Field-Effect Transistors, *Adv. Funct. Mater.*, 2014, **24**(23), 3524–3534, DOI: **10.1002/adfm.201303794**.

21 J. J. Kwok, K. S. Park, B. B. Patel, R. Dilmurat, D. Beljonne, X. B. Zuo, B. Lee and Y. Diao, Understanding Solution State Conformation and Aggregate Structure of Conjugated Polymers via Small Angle X-ray Scattering, *Macromolecules*,

2022, **55**(11), 4353–4366, DOI: **10.1021/acs.macromol.1c02449**.

22 C. M. Hansen, *Hansen solubility parameters: a user's handbook*, CRC press, 2007. DOI: **10.1201/9781420006834**.

23 J. Neu, S. Samson, K. Ding, J. J. Rech, H. Ade and W. You, Oligo(ethylene glycol) Side Chain Architecture Enables Alcohol-Processable Conjugated Polymers for Organic Solar Cells, *Macromolecules*, 2023, **56**(5), 2092–2103, DOI: **10.1021/acs.macromol.2c02259**; J. A. Emerson, D. T. W. Toolan, J. R. Howse, E. M. Furst and T. H. Epps, Determination of Solvent-Polymer and Polymer-Polymer Flory-Huggins Interaction Parameters for Poly(3-hexylthiophene) via Solvent Vapor Swelling, *Macromolecules*, 2013, **46**(16), 6533–6540, DOI: **10.1021/ma400597j**.

24 D. T. Duong, B. Walker, J. Lin, C. Kim, J. Love, B. Purushothaman, J. E. Anthony and T. Q. Nguyen, Molecular solubility and hansen solubility parameters for the analysis of phase separation in bulk heterojunctions, *J. Polym. Sci., Part B: Polym. Phys.*, 2012, **50**(20), 1405–1413, DOI: **10.1002/polb.23153**.

25 F. Machui, S. Langner, X. D. Zhu, S. Abbott and C. J. Brabec, Determination of the P3HT:PCBM solubility parameters via a binary solvent gradient method: Impact of solubility on the photovoltaic performance, *Sol. Energy Mater. Sol. Cells*, 2012, **100**, 138–146, DOI: **10.1016/j.solmat.2012.01.005**; F. Machui, S. Abbott, D. Waller, M. Koppe and C. J. Brabec, Determination of Solubility Parameters for Organic Semiconductor Formulations, *Macromol. Chem. Phys.*, 2011, **212**(19), 2159–2165, DOI: **10.1002/macp.201100284**.

26 K. F. Zhao, Q. Zhang, L. Chen, T. Zhang and Y. C. Han, Nucleation and Growth of P(NDI2OD-T2) Nanowires via Side Chain Ordering and Backbone Planarization, *Macromolecules*, 2021, **54**(5), 2143–2154, DOI: **10.1021/acs.macromol.0c02436**.

27 C. Liu, W. X. Hu, H. Q. Jiang, G. M. Liu, C. C. Han, H. Sirringhaus, F. Boué and D. J. Wang, Chain Conformation and Aggregation Structure Formation of a High Charge Mobility DPP-Based Donor-Acceptor Conjugated Polymer, *Macromolecules*, 2020, **53**(19), 8255–8266, DOI: **10.1021/acs.macromol.0c01646**.

28 B. Liu, H. Zhang, J. X. Ren, T. N. Ma, M. N. Yu, L. H. Xie and D. Lu, Effect of solvent aromaticity on poly(9,9-dioctylfluorene) (PFO) chain solution behavior and film condensed state structure, *Polymer*, 2019, 185, DOI: **10.1016/j.polymer.2019.121986**.

29 T. Li, H. Zhang, B. Liu, T. N. Ma, J. Y. Lin, L. H. Xie and D. Lu, Effect of Solvent on the Solution State of Conjugated Polymer P7DPF Including Single-Chain to Aggregated State Structure Formation, Dynamic Evolution, and Related Mechanisms, *Macromolecules*, 2020, **53**(11), 4264–4273, DOI: **10.1021/acs.macromol.0c00579**.

30 Y. F. Wang, S. Zhang, G. Freychet, Z. F. Li, K. L. Chen, C. T. Liu, Z. Q. Cao, Y. C. Chiu, W. J. Xia and X. D. Gu, Highly Deformable Rigid Glassy Conjugated Polymeric Thin Films, *Adv. Funct. Mater.*, 2023, 2306576, DOI: **10.1002/adfm.202306576**; H. Zhao, J. J. Shanahan, S. Samson, Z. Li, G. Ma, N. Prine, L. Galuska, Y. Wang, W. Xia, W. You, *et al.*, Manipulating Conjugated Polymer Backbone Dynamics through Controlled Thermal Cleavage of Alkyl Side Chains, *Macromol. Rapid Commun.*, 2022, **43**(24), e2200533, DOI: **10.1002/marc.202200533**; Z. Q. Cao, Z. F. Li, S. Zhang, L. Galuska, T. Y. Li, C. Do, W. J. Xia, K. L. Hong and X. D. Gu, Decoupling Poly(3-alkylthiophenes)' Backbone and Side-Chain Conformation by Selective Deuteration and Neutron Scattering, *Macromolecules*, 2020, **53**(24), 11142–11152, DOI: **10.1021/acs.macromol.0c02086**; S. Zhang, A. Alesadi, M. Selivanova, Z. Q. Cao, Z. Y. Qian, S. C. Luo, L. Galuska, C. Teh, M. U. Ocheje, G. T. Mason, *et al.*, Toward the Prediction and Control of Glass Transition Temperature for Donor-Acceptor Polymers, *Adv. Funct. Mater.*, 2020, **30**(27), 2002221, DOI: **10.1002/adfm.202002221**.

31 Z. Li, Y. Wang, G. Ma, Y. Liao, X. Gu and W. Xia, Probing Conformational Properties of Conjugated Polymers in Dilute Solutions Under Variable Solvent Quality via Coarse-Grained Modeling, *J. Polym. Sci.*, 2023, DOI: **10.1002/pol.20230689**, In press. W. Zhang, F. Vargas-Lara, S. V. Orski, K. L. Beers and J. F. Douglas, Modeling short-chain branched polyethylenes in dilute solution under variable solvent quality conditions: Basic configurational properties, *Polymer*, 2021, **217**, 123429, DOI: **10.1016/j.polymer.2021.123429**.

32 M. Leclerc, Optical and electrochemical transducers based on functionalized conjugated polymers, *Adv. Mater.*, 1999, **11**(18), 1491–1498, DOI: **10.1002/(Sici)1521-4095(199912)11:18<1491::Aid-Adma1491>3.0.Co;2-O**–+; S. D. D. V. Rughooputh, S. Hotta, A. J. Heeger and F. Wudl, Chromism of soluble polythienylenes, *J. Polym. Sci., Part B: Polym. Phys.*, 2003, **25**(5), 1071–1078, DOI: **10.1002/polb.1987.090250508**.

33 I. McCulloch, M. Heeney, C. Bailey, K. Genevicius, I. Macdonald, M. Shkunov, D. Sparrowe, S. Tierney, R. Wagner, W. Zhang, *et al.*, Liquid-crystalline semiconducting polymers with high charge-carrier mobility, *Nat. Mater.*, 2006, **5**(4), 328–333, DOI: **10.1038/nmat1612**.

34 A. Khasbaatar, A. Cheng, A. L. Jones, J. J. Kwok, S. K. Park, J. K. Komar, O. Lin, N. E. Jackson, Q. Chen, D. M. DeLongchamp, *et al.*, Solution Aggregate Structures of Donor Polymers Determine the Morphology and Processing Resiliency of Non-Fullerene Organic Solar Cells, *Chem. Mater.*, 2023, **35**(7), 2713–2729, DOI: **10.1021/acs.chemmater.2c02141**.

35 Z. Xu, K. S. Park, J. J. Kwok, O. Lin, B. B. Patel, P. Kafle, D. W. Davies, Q. Chen and Y. Diao, Not All Aggregates Are Made the Same: Distinct Structures of Solution Aggregates Drastically Modulate Assembly Pathways, Morphology, and Electronic Properties of Conjugated Polymers, *Adv. Mater.*, 2022, **34**(32), e2203055, DOI: **10.1002/adma.202203055**.

36 L. J. Xue, X. H. Yu and Y. C. Han, Different structures and crystallinities of poly(3-hexylthiophene) films prepared

from aged solutions, *Colloids Surf., A*, 2011, **380**(1–3), 334–340, DOI: **10.1016/j.colsurfa.2011.03.003**.

37 H. L. Yi and C. C. Hua, PBTTT-C(16) sol-gel transition by hierarchical colloidal bridging, *Soft Matter*, 2018, **14**(7), 1270–1280, DOI: **10.1039/c7sm02493b**.

38 P. S. Russo, K. A. Streletzky, A. Gorman, W. Huberty and X. Zhang, Characterization of polymers by dynamic light scattering, in *Molecular Characterization of Polymers*, Elsevier, 2021, pp. 441–498; A. Sehgal and T. A. P. Seery, Anomalous dynamic light scattering from solutions of light absorbing polymers, *Macromolecules*, 1999, **32**(23), 7807–7814, DOI: **10.1021/ma9903106**.

39 Z. Q. Cao, G. R. Ma, M. W. Leng, S. Zhang, J. H. Chen, C. Do, K. L. Hong, L. Fang and X. D. Gu, Variable-Temperature Scattering and Spectroscopy Characterizations for Temperature-Dependent Solution Assembly of PffBT4T-Based Conjugated Polymers, *ACS Appl. Polym. Mater.*, 2022, **4**(5), 3023–3033, DOI: **10.1021/acsapm.1c01511**; Y. Liu, J. Zhao, Z. Li, C. Mu, W. Ma, H. Hu, K. Jiang, H. Lin, H. Ade and H. Yan, Aggregation and morphology control enables multiple cases of high-efficiency polymer solar cells, *Nat. Commun.*, 2014, **5**, 5293, DOI: **10.1038/ncomms6293**.

40 D. R. Reid, N. E. Jackson, A. J. Bourque, C. R. Snyder, R. L. Jones and J. J. de Pablo, Aggregation and Solubility of a Model Conjugated Donor-Acceptor Polymer, *J. Phys. Chem. Lett.*, 2018, **9**(16), 4802–4807, DOI: **10.1021/acs.jpclett.8b01738**.

41 Y. C. Liao, Z. F. Li, F. Fatima and W. J. Xia, Size-dependent structural behaviors of crumpled graphene sheets, *Carbon*, 2021, **174**, 148–157, DOI: **10.1016/j.carbon.2020.12.006**; Y. Liao, Z. Li, S. Ghazanfari, F. Fatima, A. B. Croll and W. Xia, Understanding the Role of Self-Adhesion in Crumpling Behaviors of Sheet Macromolecules, *Langmuir*, 2021, **37**(28), 8627–8637, DOI: **10.1021/acs.langmuir.1c01545**; H. Arkin and W. Janke, Gyration tensor based analysis of the shapes of polymer chains in an attractive spherical cage, *J. Chem. Phys.*, 2013, **138**(5), 054904, DOI: **10.1063/1.4788616**, (acccessed 9/22/2023).